Diffusional edge enhancement observed by NMR in thin glass capillaries

D. Barsky [a,b], B. Pütz [b,c], K. Schulten [a,b,c]

[a] *Department of Biophysics, University of Illinois at Urbana/Champaign, 405 North Mathews Avenue, Urbana, IL 61801, USA*
[b] *Beckman Institute, University of Illinois at Urbana/Champaign, 405 North Mathews Avenue, Urbana, IL 61801, USA*
[c] *Department of Physics, University of Illinois at Urbana/Champaign, 405 North Mathews Avenue, Urbana, IL 61801, USA*

J. Schoeniger

Sandia National Laboratory, Livermore, CA 94551-0969, USA

E.W. Hsu and S. Blackband [1]

NMR Research Division of the Department of Radiology of Johns Hopkins University School of Medicine, 720 Rutland Avenue, Baltimore, MD 21205-2109, USA

Received 30 June 1992; in final form 16 September 1992

In NMR microscopy the effect of molecular diffusion is usually to degrade resolution and sensitivity due to destructive interference of signals from the moving spins. In samples there may exist regions that differ markedly in the translational diffusion coefficient of the molecules whose spatial distribution is being imaged, and in particular, samples may contain barriers impermeable to the translating spins. We present an experimental demonstration that, in the presence of a magnetic field gradient, a reduction in the translational mean free path of liquid molecules, due to barriers, results in the enhancement of magnetization near barriers. Monte Carlo simulations are compared with experiments. The observed effects are induced by barriers, not compartmentalization. This edge enhancement may provide a means through NMR microscopy of visualizing small impermeable structures that might otherwise be invisible.

1. Introduction

NMR microscopy has been shown to be feasible by several groups using a variety of samples (see refs. [1–19] for examples). This technique faces the same limitations on sensitivity as conventional NMR spectroscopy. In order to be able to detect signals from increasingly smaller volumes of material with increasingly greater spatial resolution, applications of NMR microscopy have been concentrated on imaging the distribution of the signal from protons in water, or other abundant, highly mobile solvent species within the system of interest.

Correspondence to: K. Schulten, Department of Biophysics, University of Illinois at Urbana/Champaign, 405 North Mathews Avenue, Urbana, IL 61801, USA.

[1] MRI Center, Hull Royal Infirmary, Hull, UK.

Because NMR imaging techniques use a magnetic field gradient for encoding spatial information, the sensitivity of NMR microscopy is less than that of NMR spectroscopy when imaging resolutions are employed that are on the order of the diffusion length of the molecules whose signal is being observed. The random diffusional displacements of different spins which originate in the same volume result is destructive interference of the oscillating magnetic fields emitted by the spins, causing loss of signal. (For a more complete discussion of diffusion and resolution in NMR microscopy, see refs. [20,21].) The characteristic diffusion length for water at room temperature is about 1 μm/ms. If the resolution is increased to the point where the loss of signal due to diffusion becomes significant, then the loss, even under optimal conditions, is proportional to the resolution and independent of the method (phase or fre-

quency encoding) used to encode spatial information [20]. The practical result is that higher resolution is gained at a cost of longer data acquisition times and smaller samples. The best resolutions achieved experimentally using NMR microscopy are currently of the order of 4 to 10 μm [3,6,7,18]. Estimates indicate that it will not be practicable to achieve imaging resolutions of higher than about one cubic micron using NMR microscopy in reasonable periods of time (see ref. [18], for example) without some unforeseen dramatic increase in the sensitivity of the technique. It would seem, therefore, unlikely that NMR microscopy could be of great utility in visualizing subcellular structures.

Most analyses of diffusion in NMR microscopy have, however, assumed that the diffusion coefficient does not vary within the sample. To be applicable to heterogeneous samples, such as cells of biological tissue, a thorough analysis of the effects of diffusion in NMR microscopy should take into account effects of variations in the translational diffusion coefficient across the sample. In particular, barriers impermeable to spins will decrease the mean free path length of molecular diffusion in the sample near the barrier. Previous theoretical analyses [22–24] indicate that this would result in relative motional narrowing of the resonances of water spins near the wall of a cylindrical capillary, which then would result in a ring of enhanced intensity in two-dimensional projection-reconstruction images of the cross section of the capillary. Some of the authors (Schoeniger, Blackband) have also experimentally observed edge enhancement effects in NMR microscopy using Fourier encoding techniques. In this Letter, we describe systematic experimental observations of diffusional edge enhancement in one- and two-dimensional Fourier encoded NMR microscopy and compare the observations with numerical simulations.

2. Theory and experimental design

The physical observable of NMR is the transverse magnetization. The magnitude $M(t)$ of the transverse magnetization of a sample of diffusing spins precessing in a magnetic field gradient decays with time according to the formula

$$M(t) = M_0 \exp(-t/T_2) \exp(-\tfrac{1}{3}\gamma^2 G^2 D t^3) , \qquad (1)$$

where the initial magnetization is assumed to be uniform, and boundary effects are ignored [25,26]. Here M_0 is the initial magnetization, T_2 is the relaxation time (relaxation in the absence of diffusion and field inhomogeneities), γ is the gyromagnetic ratio for the spins in $s^{-1}G^{-1}$, G the field gradient strength in G/cm, D the diffusion coefficient for the spins in cm^2/s, and t the time that the gradient is applied. Eq. (1) is not valid for samples where D is non-uniform. In particular, it does not apply to regions containing diffusional barriers.

In addition to diminishing signal amplitude, diffusion will also interfere with the process of frequency or phase encoding of spatial information using magnetic field gradients. In frequency encoding, diffusing spins appear to be at their average position over the readout period. In the absence of boundaries or non-uniformities in D, such averaging would be the same everywhere, and therefore not detectable. Boundaries, however, distort the averaging by a process similar to motional narrowing in NMR spectroscopy. Such distortions in the frequency response have been predicted to cause an apparent increased signal near boundaries in the transformed (image) data set, or even bright rings or bright spots, a phenomenon referred to here as motional narrowing edge enhancement (MONET) [22–24]. In principle, any frequency-encoding method employing a gradient will produce a MONET effect, although it may not be noticeable.

Eq. (1) can be derived by considering a random walk in a field gradient [27]. Although eq. (1) is not valid where D is non-uniform, a random walk argument can also be formulated in a situation of diffusional boundaries. In general, in the presence of a magnetic field gradient, spins that are initially precessing in phase will become increasingly dephased in relation to their relative displacement parallel to the gradient: the larger the displacement, the larger the dephasing. Spins near diffusional boundaries, then, are on average less displaced, and therefore less dephased. This can lead to a very high proportion of magnetization near boundaries, i.e. an edge enhancement due to a partial retention of phase coherence.

It is of practical importance that while MONET

can only appear during a readout period, the effects of translational diffusion on the microscopic distribution of the *phases* of spins precessing in a magnetic field gradient will exist whether or not that gradient is being used to encode spatial information in the sample.

An experimental NMR pulse sequence designed to study these effects may be envisioned as follows: Functionally, the experiment is divided into two independent parts. First, transverse magnetization is excited using a radio frequency (rf) pulse, and then a relatively long, relatively weak "diffusion weighting" gradient pulse G_D is applied which serves to establish a certain spatial distribution of magnetization. G_D must be such that it imparts no net phase dispersion across the sample, as would, for example, a bipolar gradient or a unipolar gradient with a 180° refocusing pulse in the middle. (Numerical simulations were employed to determine values of gradient strength and durations which should produce a noticeable edge enhancement.) Next, a sequence of gradient pulses is applied which encodes information about the spatial distribution of the magnetization. The observation pulse sequence should have the property that the spatial information should be encoded and recorded in a brief time period, in order that the effects of diffusion on the magnetization during that period be minimal. For this we have used a fast gradient echo sequence.

This experimental design has the advantage that, in contrast to MONET, the readout gradient is not required to both encode spatial information and produce an edge effect. Since it takes time for the differential attenuation of spins near versus far from boundaries to produce markedly different magnetizations, a signal will be affected by MONET only after there has been a great deal of phase dispersion across the sample due to the frequency encoding gradient, and, therefore, after the signal has become very weak. In the experiment we describe above, the gradient area (product of gradient strength and duration, equivalent to the maximum radius reached in reciprocal space) needed to produce the edge effect may be much larger than that needed to encode the image information to a reasonable resolution. In the experiments presented here, the difference was about a factor of two. This makes it difficult in practice, then, to obtain an adequate signal to noise ratio to observe MONET; nevertheless, preliminary studies in our lab indicate that in careful experiments such an effect does occur.

3. Experimental methods

Imaging studies were performed using a homebuilt imaging probe, consisting primarily of a set of quadrupolar field gradients and a 1.5 mm diameter 5-turn solenoidal receiver/transmitter coil supported in a novel concentric tuning assembly [20]. The axis of the radio frequency (rf) solenoid (Y direction) is perpendicular to the direction of the static (Z) magnetic field. The probe is capable of producing 21.5 G/cm A in the Y direction and greater than 90 G/cm A in the X and Z directions. Gradient switching times are less than 10 μs. The probe is interfaced with a Bruker AM-360 8.5 T spectrometer sited at Johns Hopkins Hospital in Baltimore, Maryland. The spectrometer is equipped with microimaging accessories, including gradient and rf waveform boards, a linear rf amplifier, gradient power supplies, and image display capabilities.

Samples consisted of glass capillary tubes filled with water, Capillaries used in this experiment were either 600 or 190 μm in diameter. The smaller diameter tube was formed by heating and pulling one of the larger tubes, and its diameter determined by imaging its water filled cross section.

The two-part pulse sequence is shown in fig. 1. Diffusion weighting is first applied along a direction perpendicular to the axis of the capillary using a carefully balanced, relatively long, relatively weak gradient pulse of total duration 2τ, with a 180° rf pulse applied in the middle of the gradient after time τ.

Spatial information was encoded separately using a brief, strong frequency-encoding gradient pulse (and intense phase-encoding gradient pulses in 2DFT experiments) that is defocused by gradient reversal prior to data acquisition and centered about the spin echo. For the data used in this Letter, the dephasing lobe of the gradient echo was −122.5 G/cm for 0.98 ms, and the readout lobe was 49 G/cm for 5.12 ms, yielding an imaging resolution of approximately 9.4 μm. For diffusion weighting, we used values of 2τ between 20 and 70 ms in increments of 10 ms with

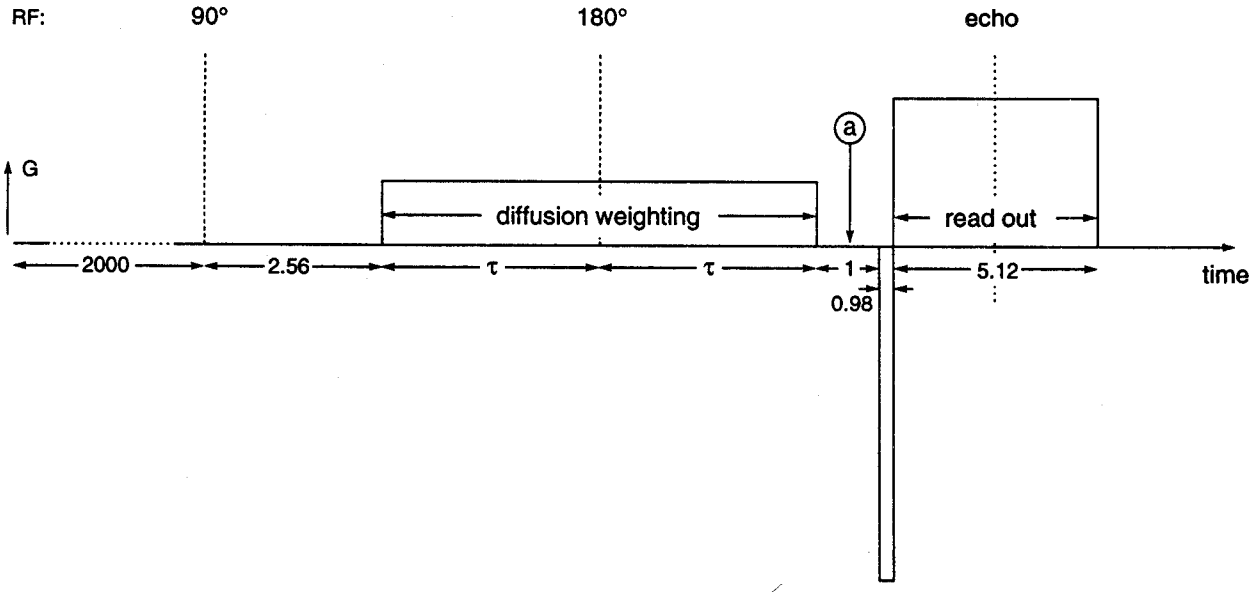

Fig. 1. The pulse sequence used in the experiments reported in this Letter and investigated using numerical simulations. Radiofrequency (rf) pulses are indicated by vertical dashed lines and the tip angle is given in deg. Magnetic field gradient pulses are indicated by rectangles. The diffusion weighting gradient was applied in the same direction across the sample as the frequency encoding gradient. The areas on either side of the 180° pulse were precisely balanced by first exactly centering the gradient echo in the absence of the weighting gradient, and then turning on the weighting gradient and carefully adjusting the timing of the refocusing pulse in order to recenter the echo. This procedure allowed the authors to compensate for the fact that the time course of the gradient rise and fall are not identical, and ensured that none of the observed effects are due to asymmetric sampling of reciprocal space. The refocusing 180° pulse had a duration of 23 μs, so that resonant offset effects were negligible.

gradient strengths G of 3.7, 4.9, 5.4, 6.1, 7.4, 8.6 G/cm. Each data set acquired was the average of 64 scans with a relaxation delay (TR) of 2 s.

Two-dimensional imaging was performed using two-dimensional Fourier encoding [28,29] where the phase encoding pulse was applied immediately prior to the dephasing lobe of the gradient echo pulse. Two-dimensional data sets were formed by averaging two sets of scans, each with 128 phase gradient increments of 0.5 G/cm per increment, and a relaxation delay (TR) of 3 s between scans. The duration of the phase gradient was 2.56 ms. The diffusion weighting gradient used had a strength 4.9 G/cm with a total duration of 40 ms.

For one-dimensional profiles, 128 complex data points were collected, and for two-dimensional images, 128 phase encoding steps were employed, creating a 128×128 point complex data set. One-dimensional or two-dimensional magnetization distributions were reconstructed using the appropriate one- or two-dimensional discrete Fourier transform without digital filtering. One-dimensional images were recorded with and without slice selection; two-dimensional images were recorded with slice selection.

Monte Carlo techniques for numerical simulations of diffusing spins precessing in a magnetic field gradient are described in ref. [23]. These simulations allow us to obtain the magnetization in any region as the vector sum of all of the magnetic moments within that region. Magnetization profiles produced by complex gradient time courses in nearly arbitrarily shaped cavities can be simulated with this technique.

Simulations were employed in the design of experiments and in the analysis of experimental results. By simulations we were able to look for experimental parameters that would result in the greatest edge enhancement and to evaluate the effect of the readout pulse sequence on the diffusion weighting. To this end, we examined by simulation the spatial distribution of magnetization at time a in

fig. 1. Such magnetization profiles were then compared with Fourier transforms of the FID signal, acquired by a simulated pulse sequence. We found that the rapid defocusing and readout gradients did not noticeably distort the magnetization profiles.

4. Results

4.1. Experimental

Fig. 2 displays experimental and simulated magnetization profiles measured as a function of the diffusion weighting gradient strength G_D for two different capillary diameters. For $2\tau = 50$ ms, with gradients considerably weaker than 3.7 G/cm, the shape of the profile does not deviate significantly from the unweighted parabolic one-dimensional projection of the cylinder of water. For gradients considerably stronger than 5.4 G/cm no discernible information remains after the diffusion weighting.

Smaller τ values increase the acceptable range of G_D, and we observe the τ dependence of edge enhancement in a second set of experiments. The results are presented in table 1 where they are characterized by two ratios: the edge peak height divided by the center height C, and the edge peak height divided by the edge valley height V (unity if no edge peak exists). There are three possibilities: (1) If $C < 1$ and $V \approx 1$, then the profiles are hardly distorted from a parabola. Even slight distortions, however, may give rise to rings if a filtered back-projection is used for reconstruction [22]. (2) If $C \approx 1$ and $V > 1$, then sharply discernible peaks are visible but of lower intensity than the center. (3) If $C > 1$ and $V > 1$, then edge peaks are both sharp and intense. Profiles which were only very weakly distorted are marked by a "–" symbol. In this second set of observations, many profiles were unsymmetric about the center, and this is reflected in the high uncertainties. Importantly, however, even reconstructions created from distorted profiles show a clear, bright edge enhancement. Characterizations of the observations and simulations in fig. 2 have been included in table 1 for reference.

In order to ensure that the observed profiles are not distorted by sample misalignment of rf inhomogeneities along the length of the coil, we also recorded profiles of a slice along the axis of the tube obtained by using a selective 90° excitation pulse in the presence of a magnetic field gradient along the axis of the tube. Other than the expected loss of signal, the magnetization profile of a 0.6 mm slice was identical to the profile obtained using a non-selective 90°-pulse in which case the excitation profile along

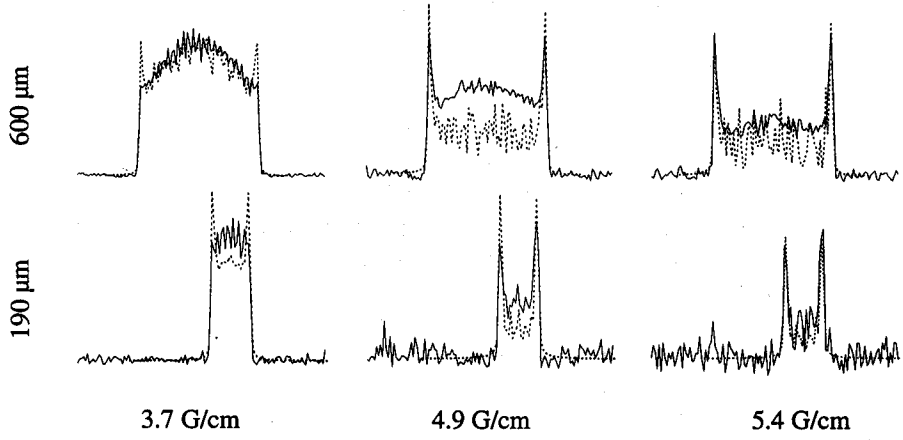

Fig. 2. Observed (solid) and simulated (dotted) magnetization profiles by Fourier transform (absolute value) of the FID signal after diffusion weighting of duration $2\tau = 50$ ms. The columns present the gradient strengths $G_D = 3.7$, 4.9 and 5.4 G/cm (left to right); the rows present two capillary diameters: 600 μm (upper row) and 190 μm (lower row). The profiles are the real channel of an unfiltered DFT of the gradient echo signal; the amplitudes have been normalized. Cf. corresponding rows of table 1 for 600 μm diameter.

Table 1
Characteristic ratios of observed magnetization profiles of a 600 μm capillary as a function of G_D (columns) and 2τ (rows), as defined in the text and in the form C/V. The simulation results (marked by "sim.") correspond to the upper row of profiles in fig. 2

2τ (ms)	G_D (G/cm)					
	3.7	4.9	5.4	6.1	7.4	8.6
20					–	–
30		–		0.5/1.0±0.1/0.1	0.6/1.0±0.2/0.1	0.6/1.0±0.1/0.1
40	–	0.6/1.0±0.2/0.1		0.9/1.3±0.1/0.3	1.6/2.2±0.3/0.3	3.5/3.5±0.8/0.8
50	0.5/1.0±0.2/0.2	1.3/1.6±0.2/0.3	2.3/2.9±0.1/0.2	4/4±0.2/0.2	8/8±2/2	>4/>4
50 sim.	1.0/1.9±0.1/0.2	2.9/3.6±0.7/0.6	3.0/3.8±0.9/1.7			
60	1.3/1.6±0.2/0.1	6/6±2/2				
70	4/4±0.1/0.1					

the tube is nearly a Gaussian with a width of 1.2 mm at half-height.

We have predicted that edge enhancement should appear as a bright edge in an image. We therefore produced cross sectional images of a 600 μm capillary tube filled with water. On each scan, the transverse magnetization was diffusion weighted using a gradient pulse as described in section 3. The resulting images are shown in fig. 3. Edge-enhancement effects can be clearly seen as bright crescents at the margins of the tube. In follow-up experiments we verified that the location of the crescents depends only on the orientation of the diffusion weighting gradient. Indeed, when we rotated the diffusion weighting gradient by 90°, i.e. perpendicular to the readout gradient, we found bright crescents perpendicular to the readout gradient. We conclude that the edge enhancement is not an artifact of the methods

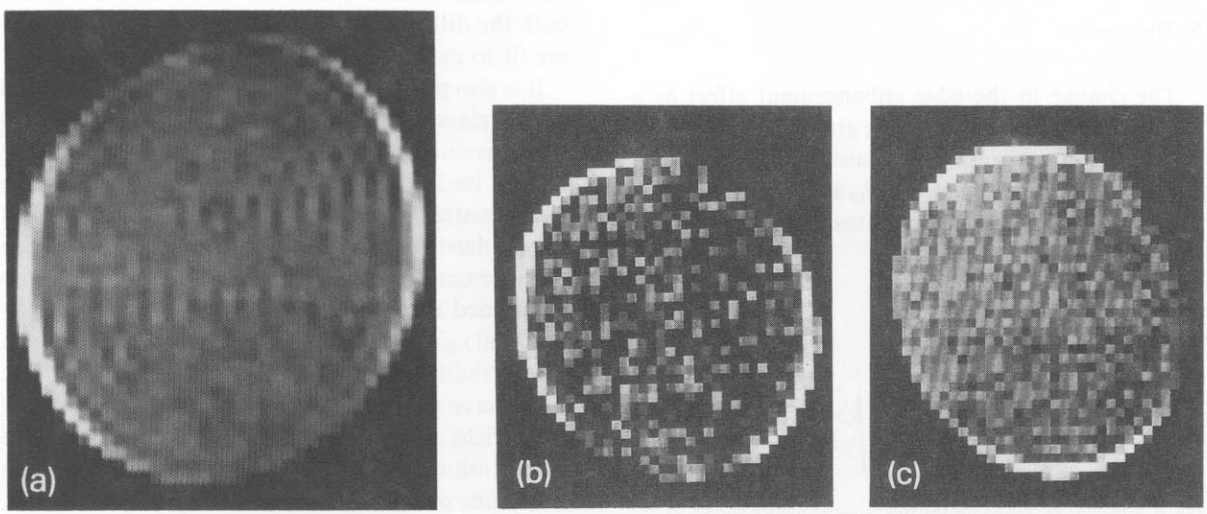

Fig. 3. Fourier encoded cross-sectional images of a 600 μm internal diameter glass tube filled with water. In all images the frequency encoding gradient was applied horizontally, and the phase encoding gradient vertically. The bright crescents are the result of diffusional edge enhancement. The diffusion weighting gradient was applied in the same direction as the frequency encoding gradient in (a) and (b). In image (c) the gradient was applied in the direction of the phase encoding gradient. The single image at left (a) and the pair of images at right (b) and (c) were observed in two separate experiments, and were processed differently. In images (b) and (c) the sign of the dephasing and readout gradients was flipped from that shown in fig. 1, eliminating the Gibbs ringing seen in image (a) and in the weakest gradient profiles of fig. 2.

chosen for data collection of processing.

4.2. Theoretical

In accordance with experimental observations, the numerical simulations were quite sensitive to the choices of G_D, τ, and, additionally, the self-diffusion coefficient of water D. Using values that coincide with the experiments and $D=2.3\times10^{-5}$ cm^2/s, we have found reasonable agreement (cf. fig. 2), but the characteristic ratios (as presented in table 1) of the simulation results are $1.0/1.9\pm0.1/0.2$ while the experimental results yield $0.5/1\pm0.2/0.2$. Excellent fits could be found for smaller D, as shown in fig. 4. For $D=1.63\times10^{-5}$ cm^2/s the characteristic ratios are $0.6/1.1\pm0.03/0.03$, in close agreement with experiment. The significance of such a low value of D is not yet known (see also section 5).

On the left-hand side of fig. 4 we observe that the τ dependence by simulation has the same character as that of the experiments. The characteristic ratios are $1.0/1.9\pm0.1/0.2$, $0.6/1.1\pm0.1/0.1$ and $0.34/1.0\pm0.02/0.01$ from top to bottom.

5. Discussion

The change in the edge enhancement effect as a function of diffusion weighting gradient strength G_D and duration τ argues against susceptibility artifacts, as does the replication of the G_D and τ dependencies by simulations. What is more, imaging artifacts, such as sample orientation, have been excluded by switching the orientation of the diffusion weighting gradient.

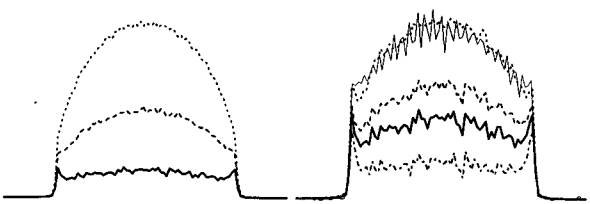

Fig. 4. Simulation results for the full pulse sequence shown in fig. 1 for a capillary diameter of 600 μm with $G_D=3.7$ G/cm. Right: Effect of the self-diffusion coefficient D for water, where $D=1.6$, 2.0, 2.3, 3.0×10^{-5} cm^2/s from top to bottom with $2\tau=50$ ms. We have overlayed (light solid line) the corresponding experimental result of fig. 2. Left: Effect of diffusion weighting time τ with $D=2.3\times10^{-5}$ cm^2/s where $2\tau=30$, 40, 50 ms from top to bottom. Left and right heavy solid curves are identical except for scale.

The ratio of edge to center intensity is very sensitive to the choice of gradient strengths and timings. One may observe, in the figures and table, that the edge-enhancement effect is less sensitive to the diffusion coefficient D than to the gradient strength G_D and most sensitive to the diffusion weighting duration τ. This can be understood through eq. (1), where these terms appear in the exponent in sequentially increasing powers.

It has already been mentioned that the simulations have resulted in peaks that are sharper (i.e. have larger characteristic ratios) than the corresponding experiments. Simulations can be made to fit the experimental results by lowering the self-diffusion coefficient of water, as seen in fig. 4, but there is no physical justification for this. On the other hand, an enhanced relaxivity of the glass walls seems plausible. Additional experiments could be undertaken to test this, perhaps by adsorbing paramagnetic metal ions onto the glass capillary walls, in order to saturate any ion binding sites on the walls of the tube. Furthermore, simulations could be performed where both the diffusion coefficient and the wall relaxivity are fit to experimental data.

It is also possible that the susceptibility differences of air, glass, and water could give rise to field inhomogeneities near the capillary walls which could, in turn, lead to enhanced relaxation at the edges – an effect contrary to edge enhancement. Such an effect may indeed play a small role in reducing the edge enhancement, perhaps alongside the wall relaxivity mentioned above. For a perfectly cylindrical (or ellipsoidal) glass capillary, however, the differences in susceptibility between air and glass, and glass and water have no effect on the shape and homogeneity of the field in the water which fills the capillary. The susceptibility differences serve only to modify the amplitude of the field inside the capillary walls and, in fact, negligibly so – on the order of a few ppm. This can be verified by a straightforward magnetostatics calculation [30].

On the other hand, imperfections in the surface of the capillary walls can lead to significant, yet short-ranged inhomogeneities. Consider a small, say one μm high, glass bump in the capillary surface. The

bump, to first order, produces a dipolar field distortion. Magnetostatics shows that this can produce a maximum field difference on the order of 1000 G/cm across the surface. A water spin passing through such an inhomogeneity can be additionally relaxed by about 13%, as given by the Hahn–Torrey term, yet the dipolar field causes negligible relaxation for spins more than a micron or two away from the bump, since it is the square of the gradient of a dipolar field which enters into the Hahn–Torrey term, and this gives a r^{-8} dependence to the relaxation induced by the bump where r is the distance from its center [31]. Thus, small irregularities in the glass capillary walls can induce large, but very short-ranged, magnetic field inhomogeneities. Since water spins experience a net displacement of about one micron in a millisecond, not all spins may be expected to get within a micron of the walls in 60 ms, but spins already in the vicinity of the walls can experience some extra relaxation. Nevertheless, as we observe experimentally, this does not eliminate the boundary-induced phase coherence which produces visible edge enhancement.

Finally, we emphasize that the edge-enhancement effect is not due to compartmentalization. It would also occur at a boundary between two infinitely extended distribution of spins.

6. Conclusion

Systematic experimental observations of the theoretically predicted effect of edge enhancement in NMR microscopy due to restricted diffusion at boundaries are reported here for the first time. This is a potential technique for contrast enhancement in NMR microscopy, and may provide a means for detecting boundaries in NMR micrographs, even when the actual boundaries themselves cannot be resolved.

We have demonstrated, both experimentally and theoretically, that under suitable conditions, a bipolar gradient pulse may be used to annihilate any magnetization which is not immediately next to a boundary. In addition to applications in imaging, this effect could potentially be exploited to study a variety of processes occurring in inhomogeneous liquid/solid samples, such as surface-catalyzed chemical reactions, relaxivity of surfaces, or mobility of spins near surfaces, because it allows one to obtain a spectroscopic signal from only those spins near surfaces – the nearness depending on the diffusion coefficient of the bulk liquid and the gradient strength and duration employed in the pulse sequence. The effect should not only occur near impermeable barriers, but any region of abrupt transition in diffusion coefficient. This letter provides the understanding needed to avoid such effects where they are not desired, as well as to exploit edge-enhancement effects for imaging microscopic structures in tissues and biological samples, such as bone matter, cells, or possibly even cell organelles.

Acknowledgement

This work has been completed at the Resource for Concurrent Biological Computing at the University of Illinois with the funding of the National Institutes of Health (grant P41RR05969). The NMR experiments have also been supported by NIH (Grant R29CA45308). We have profited greatly from the use of the computer facilities at the National Center for Supercomputing Applications. DB is supported by an NIH training grant, EH holds a Howard Hughes predoctoral fellowship.

References

[1] P. Mansfield and P. Grannell, Phys. Rev. B 12 (1975) 3629.
[2] P.C. Lauterbur, IEEE Trans. Nucl. Sci. NA-31 (1984) 4.
[3] K. Hedges, Ph.D. Thesis, Stonybrook University (1984).
[4] R.A. Meyer and T.R. Brown, J. Magn. Reson. 76 (1988) 393.
[5] G.A. Johnson, M.B. Thompson, S.L. Gewalt and C.E. Hayes, J. Magn. Reson. 68 (1986) 129.
[6] G.P. Coffer, J.M. Brown and G.A. Johnson, J. Magn. Reson. 83 (1989) 129.
[7] J.B. Aguayo, S.J. Blackband, J. Schoeniger, M.A. Mattingly and M. Hintermann, Nature 322 (1986) 190.
[8] J.B. Aguayo, S.J. Blackband, J.P. Wehrle, J.D. Glickson and M.A. Mattingly, Ann. NY Acad. Sci. 508 (1987) 399.
[9] L.W. Hedlund, G.A. Johnson and G.I. Mills, Invest. Radiol. 21 (1988) 843.
[10] J.C. Chatham, S. Ackerman and S.J. Blackband, Magn. Reson. Med. 21 (1991) 144.
[11] F.W. Wehrli, S.I. Wehrle and J. Williams, Radiology 177(P) (1990) 187.

[12] M. Asdente, L. Pavesi, P. Oreste, A. Colombo, W. Kuhn and E. Tremoli, Atherosclerosis 80 (1990) 245.
[13] J. Bitoun, H. Saint-Jalmes, B.G. Querleux, L. Darrasse, O. Jolibet, I. Idy-Peretti, M. Wartski, S.B. Richard and J.L. Leveque, Radiology 176 (1990) 457.
[14] C.D. Eccles and P.T. Callaghan, J. Magn. Reson. 68 (1986) 393.
[15] A. Conelly, J.A.B. Lohman, B.C. Loughman, H. Quiqapoix and R.G. Ratcliffe, J. Exp. Bot. 38 (1987) 1713.
[16] J.M. Brown, J.F. Thomas, G.P. Coffer and G.A. Johnson, Bot. Gaz. 149 (1988) 253.
[17] L. Sillerud, J. Freyer, M. Neeman and M. Mattingly, Magn. Reson. Med. 16 (1990) 380.
[18] Z.H. Cho, C.B. Ahn, S.C. Juh, H.K. Lee, R.E. Jacobs, S. Lee, J.H. Yi and J.M. Jo, Med. Phys. 15 (1988) 815.
[19] R. Bowtell, G. Brown, P. Glover, M. McJury and P. Mansfield, Phil. Trans. P. Soc. London A 333 (1990) 457.
[20] J.S. Schoeniger, Ph.D. Thesis, The Johns Hopkins University (1992).
[21] P.T. Callaghan, Principles of NMR microscopy (Oxford Univ. Press, Oxford, 1991).
[22] B. Pütz, D. Barsky and K. Schulten, Chem. Phys. Letters 183 (1991) 391.
[23] B. Pütz, D. Barsky and K. Schulten, J. Magn. Reson. 97 (1992) 27.
[24] W.B. Hyslop and P.C. Lauterbur, J. Magn. Reson. 94 (1991) 501.
[25] E.L. Hahn, Phys. Rev. 80 (1950) 580.
[26] H.C. Torrey, Phys. Rev. 104 (1956) 563.
[27] H.Y. Carr and E.M. Purcell, Phys. Rev. 94 (1954) 630.
[28] A. Kumar, D. Welti and R.R. Ernst, J. Magn. Reson. 18 (1957) 69.
[29] W.H. Edelstein, J.M.S. Hutchinson, G. Johnson and T. Redpath, Phys. Med. Biol. 25 (1980) 751.
[30] K.M. Lüdeke and P. Röschmann and R. Tischler, Magn. Reson. Imag. 3 (1985) 329.
[31] W.R. Bauer and K. Schulten, Magn. Reson. Med. 26 (1992) 16.